Narrowband Optical Coupler Using Fano Interference in First Order Diffraction

Giorgio Quaranta, Fabian Lütolf, Olivier J. F. Martin, and Benjamin Gallinet*

ACCESS | Metrics & More | Article Recommendations | SI Supporting Information

ABSTRACT: Light coupling in waveguides has been extensively investigated in a variety of contexts, from photonic integrated circuits to biosensing and near-eye displays for augmented reality. Here, narrowband diffraction is reported using a Fano interference effect in hybrid nanostructures. The excitation of hybrid plasmonic and bulk waveguides allows for a selectivity of 10 nm bandwidth in the first order and strong reduction of the entire zeroth order. A Fano formalism is used to predict the maximal diffraction efficiency at critical coupling, when external mode coupling balances intrinsic losses. It is found that the first order and zeroth order are related by a Fano-like spectral profile with similar spectral widths, resonance wavelengths, and modulation depths and differ only in the asymmetry parameter. The diffraction efficiency, angle, and wavelength can be solely tuned by the thin film thickness. A semianalytical dispersion model of the hybrid system is introduced and validated experimentally. Applications are foreseen in many optical devices that require color-selective coupling or dispersive properties such as optical document security or near-eye displays. The dispersion behavior under a divergent light source can also be utilized to design inexpensive, compact, and robust spectrometers or biosensors.

KEYWORDS: *narrowband diffraction, optical coupler, resonant waveguide grating, Fano resonance, guided mode resonance, plasmon*
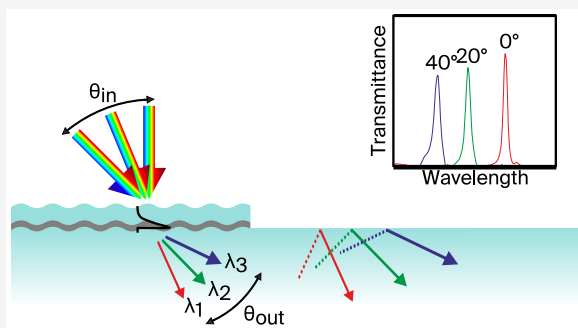
L ight coupling into waveguides has been instrumental to the development of telecommunication systems and photonic integrated circuits, for which various approaches have been investigated.[1] Grating couplers have become standard solutions thanks to their ability to efficiently bend light and later to their efficient manufacturing by lithographic methods.[2−4] Resonant waveguide gratings (RWGs) consist of a waveguide with a periodic corrugation.[5] In particular, they have been primarily used as couplers in thin film waveguides, and later as filters in the zeroth order of diffraction. Similar effects of guided mode resonances (GMRs) have also been reported in photonic crystals.[6] Periodic metallic structures, for example under the form of nanohole arrays[7,8] or corrugated thin films,[7,9] enable light coupling into propagating surface plasmons. Similarly to RWGs, the use of zeroth order diffraction has been implemented in plasmonic filters for imaging devices.[10] A large range of applications of guided mode and plasmonic resonances has been found in biosensing thanks to the high sensitivity of the modes to local perturbation of their environment.[5,11]

When the thickness of the waveguide is increased to very large dimensions compared to the wavelength, the mode distribution approaches that of a continuum and the system is referred as a multimode light guide. Grating coupling into a multimode light guide can be achieved if the diffraction angle is larger than the total internal diffraction angle, an approach widely used for augmented reality optical combiners.[12] Among

grating couplers in multimode light guides, approaches based on slanted gratings,[13] oblique coatings[14] or metasurface-based designs have been implemented.[15−17] The main challenge is the optimization of first order diffraction in transmission over a broad range of incidence angles, while achieving total internal reflection in the substrate. Sophisticated optimization methods based on genetic algorithm, topology optimization, and neural networks have allowed significant improvements in their diffraction efficiency,[18] which can reach for example up to 80% with unpolarized light from normal incidence to 75° diffracted angle.[19] When used in first order diffraction, these nanostructures show naturally a broadband dispersion and an additional signal in the zeroth order. This effect can be detrimental for applications where a good spectral demultiplexing is sought and its mitigation remains challenging by pure geometrical optimization of existing devices.

Therefore, an approach where resonances are observed only in the first order of diffraction would overcome these limitations. Resonant metasurfaces for light deflection in
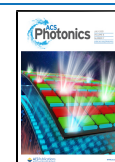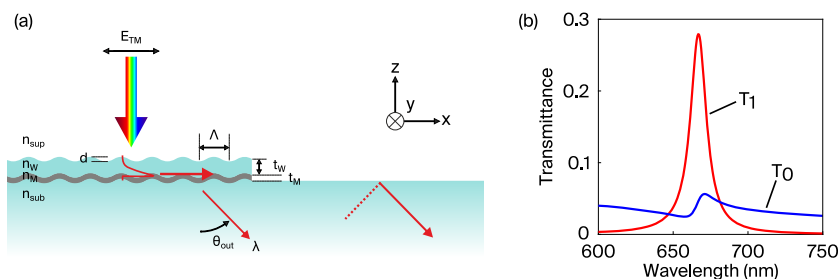
Figure 1. (a) Schematic of the device which allows to couple TM-polarized light with high wavelength selectivity into a thick multimode waveguide. The wavelength range, as well as the coupled angle θ_{out}, can be independently tuned by changing geometrical parameters of the device (i.e., the grating period Λ and the thickness of the dielectric waveguide t_W). (b) Simulated efficiencies T_0 and T_1 for $\Lambda = 500$ nm, $d = 20$ nm, $t_W = 80$ nm, $t_M = 50$ nm, showing a peak in the first diffraction order with full width half-maximum of 10 nm.

transmission have been reported with very high quality factors based on the use of GMRs and quasibound states in the continuum.[20−22] GMRs appear in a variety of photonic and plasmonic systems. When their quality factor is high, they are associated with a Fano interference, resulting from their interaction with the continuum of reflected, transmitted, or diffracted light.[5,23−25] Thus, a deep understanding of the Fano effect in GMR devices is instrumental to the design of narrowband diffractive elements, couplers, and metasurfaces.

In this work, we report on resonant corrugated waveguides performing diffraction in a multimode light guide substrate with a 10 nm bandwidth. This is achieved by a Fano interference effect between hybrid plasmonic−dielectric waveguide modes and the continuum of diffracted light in the first order. The use of metallic structures also allows a quasisuppression of the off-resonant amplitude. An analysis of the mode dispersion and coupling shows that an energy balance in the guided mode, when optical coupling equals optical losses, yields a maximal first order intensity. We also show that the dielectric waveguide thickness can directly control the direction of the diffracted beam, a degree of freedom additional to the well-known grating period. In the following, we will investigate the mechanisms of coupling, propagation into the corrugated waveguide, and release in the multimode light guide using a semianalytical model. The waveguide mode dispersion will be derived and compared to numerical simulations, as a function of dielectric and metallic layer thicknesses. The mode coupling and energy storage will be analyzed in terms of a Fano interference formalism to find the film thickness parameters maximizing the first order diffraction while minimizing the zeroth order transmission. Devices will be fabricated with UV nanoimprint lithography and thin film coatings, their diffraction efficiency spectrum measured and compared to the modal dispersion model. Finally, we will illustrate how the angular dependency of the structure reduces the light divergence after diffraction, which can be used for example in compact spectrometer devices.

RESULTS AND DISCUSSION

The concept of narrowband first order diffraction presented here is based on the excitation of surface modes of a dielectric waveguide with a thin metallic substrate.[26,27] A schematic of such a structure is shown in Figure 1a.

At resonance, the incident TM-polarized light (with magnetic field parallel to the y-axis) is coupled from the air superstrate into surface modes at the corrugated dielectric−metallic interface of the waveguide. The waveguide corrugation is characterized by a grating of period Λ and a modulation

depth d. Light is evanescently transmitted to the other metallic interface and radiated into the multimode substrate as a guided mode. As detailed below, it interferes with the continuum of light directly diffracted in the first order of transmission T_1, resulting in a Fano-like intensity profile as measured in Figure 1b. Two other optical paths are available, which we aim to minimize in this work: the direct transmission in the zeroth order, and the light resonantly incoupled and outcoupled into the zeroth order of transmission. These two paths also interfere in a Fano-like fashion in the zeroth order of transmission T_0. The spectral full-width at half-maximum (fwhm) of the first order diffraction efficiency is approximately 10 nm, which is very low for a plasmonic structure. This is a consequence of the hybrid plasmonic−dielectric nature of the waveguide modes. On the other hand, the zeroth order transmission is weak across the spectral window under investigation and carries an asymmetric line shape around the resonance, typical of a Fano interference. Thus, it appears that the same resonance carries two different spectral signatures, whether the zeroth or first order of diffraction is considered.

We first investigate the modal structure of the system using a semianalytical model and numerical simulations. In the following, we refer to the thicknesses of the dielectric waveguide and metallic layers as t_W and t_M, respectively. The refractive indices of the superstrate, dielectric layer, metallic layer and multimode waveguide substrate are n_{sup}, n_W, n_M, and n_{sub}, respectively. Without the dielectric waveguide ($t_W = 0$), the configuration is the well-known metallic film capable of supporting surface-plasmon polaritons (SPPs).[26,28] When a dielectric layer of thickness t_W is added to the plasmonic waveguide, bulk and surface modes can be excited.[27] Considering a grating depth d well below the wavelength, interfaces are assumed to be flat and the dispersion relation can be calculated semianalytically by imposing the continuity of the wave equation for E_x and H_y at the two interfaces for TM polarization:

$$\tanh(k_W t_W) = -\frac{A \tanh(k_M t_M) + B}{C \tanh(k_M t_M) + D} \tag{1}$$

where the four coefficients are

$$
\begin{aligned}
A &= k_W n_W^2 (k_M^2 n_{sup}^2 n_{sub}^2 + k_{sup} k_{sub} n_M^4) \\
B &= k_W k_M n_W^2 n_M^2 (k_{sup} n_{sub}^2 + k_{sub} n_{sup}^2) \\
C &= k_{sub} k_W^2 n_M^4 n_{sup}^2 + k_{sup} k_M^2 n_W^4 n_{sub}^2 \\
D &= k_M n_M^2 (k_W^2 n_{sup}^2 n_{sub}^2 + k_{sub} k_{sup} n_W^4)
\end{aligned}
\tag{2}
$$
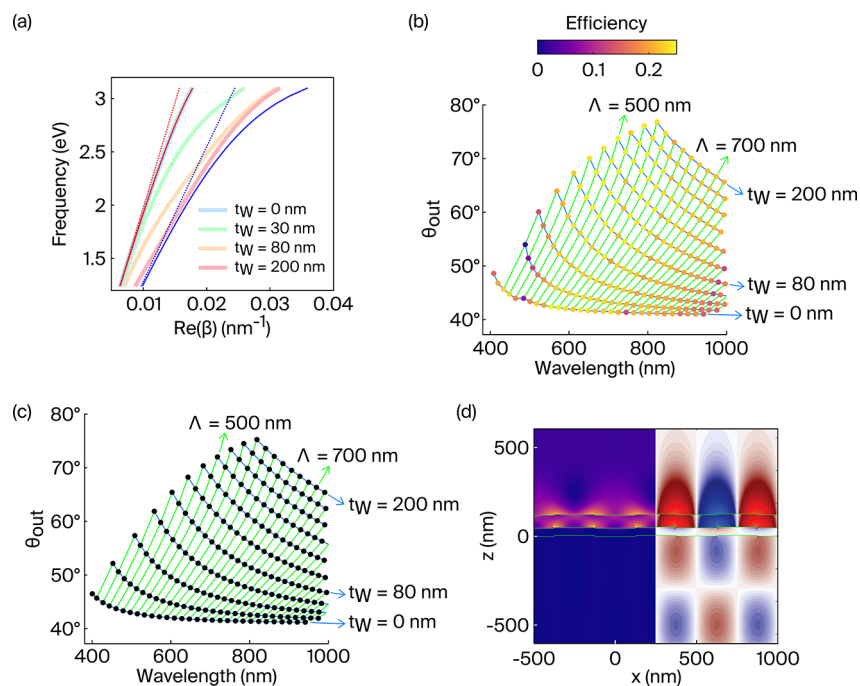
Figure 2. (a) Dispersion relations for the hybrid plasmonic–dielectric modes (pastel lines), for different waveguide thicknesses t_W. Dashed red and blue lines correspond to light lines of air and SiO_2, respectively. Solid red and blue lines correspond to SPP modes for the single air/Ag interface and SiO_2/Ag interface, respectively. (b) Simulated efficiency T_1 for the first diffraction order transmitted field at its peak, as a function of the grating period Λ and the waveguide thickness t_W. The green and blue lines connect geometries with the same grating period Λ and the same waveguide thickness t_W, respectively. The other parameters are $d = 13$ nm, $t_M = 50$ nm. (c) Calculated positions of the first order transmitted diffracted field at its peak, for the cases of (a) using the dispersion relation (eq 1). (c) RCWA simulations at $\lambda = 663$ nm, $\Lambda = 500$ nm, $t_W = 80$ nm, $t_M = 50$ nm. Left simulation: electric field intensity $|\mathbf{E}|^2$. Right simulation: $\mathrm{Re}[E_z/E_0]$ field.

where $k_i \equiv k_{z,i} = \sqrt{\beta^2 - n_i^2 k_0^2}$ is the component of the wavevector perpendicular to the interface in the different media (i = sup, W, M, sub), and $k_0 = 2\pi/\lambda$ is the wavevector of the propagating wave in a vacuum, and β is the complex propagation vector parallel to the surface. In the following, the superstrate is air ($n_{sup} = 1$), the dielectric layer, and the multimode substrate are chosen to be silica (SiO_2), modeled with dielectric function from Malitson[29] and the metallic layer is silver (Ag), with dielectric function from Yang et al.[30] Because of the complex refractive index n_M, the propagation constant β has complex values, and thus the mode distributions of a dielectric waveguide with a metallic substrate are different compared to the case of a pure dielectric waveguide. We are interested at the TM_0 mode: it has no cut-off condition and is partly confined at the metal–waveguide interface,[27] as illustrated in Figure 2d.

In particular, the modal electric field intensity $|\mathbf{E}|^2$ shows hot spot regions of high field confinement at both metal/dielectric and dielectric/air interfaces. The real part of the electric field in z-direction indicates the presence of surface charges at the dielectric/metal interface, the signature of a plasmon mode. The dispersion curves derived from eq 1 are shown in Figure 2a. In the case of $t_W = 0$, the dispersion relation is reduced to the dispersion relation of a metallic layer with air-Ag interface.[26] As the dielectric waveguide thickness t_W is increased, the amplitude of the propagation wavevector is increased further. In case of large thicknesses t_W and t_M the dispersion curve approaches the curve of the SPP mode at SiO_2–Ag interface.

Figure 2b reports the peak position of first order diffraction efficiency, peak wavelength and diffraction angle for different

grating periods Λ and waveguide thicknesses t_W. The calculations are performed with rigorous coupled-wave analysis (RCWA),[31] which can be used in this context with a large enough number of Fourier harmonics.[32−34] The corresponding calculations with the semianalytical model of eq 1 is plotted in Figure 2c: the average difference between the computed resonance wavelengths and those extracted from the semi-analytical model (eq 1) is around 0.7%, thus showing a very good agreement. The system without the dielectric waveguide layer also shows wavelength selectivity in first order diffraction. With air as superstrate, Ag as metallic layer and SiO_2 as multimode waveguide substrate, the coupled angle θ_{out} is near the total internal reflection (TIR) angle for the SiO_2 substrate, which is around 42°. However, the coupled angle is very weakly influenced by the grating periodicity. The green lines represent different grating periods, equispaced from the left ($\Lambda = 340$ nm) to the right ($\Lambda = 940$ nm). Without the dielectric waveguide layer, the diffraction angle ranges from 42° to 48° for the range of periods Λ investigated ($t_W = 0$ nm, along the bottom blue line). Inspecting the peak position along the green lines, we observe that the waveguide layer gives an additional degree of freedom to the system. Most importantly, the thickness t_W of the dielectric waveguide layer drastically influences the peak position, shifting for example from 42° ($t_W = 0$ nm) to 75° ($t_W = 200$ nm) for $\Lambda = 560$ nm. Thus, a device with the additional dielectric waveguide layer can operate in a significantly higher range of coupled angles θ_{out}. The highest efficiencies are obtained between 600 and 800 nm, for which the coupling conditions in the waveguide mode are optimized. The fluctuations of the efficiencies are simulation artifacts related to the layers discretization.
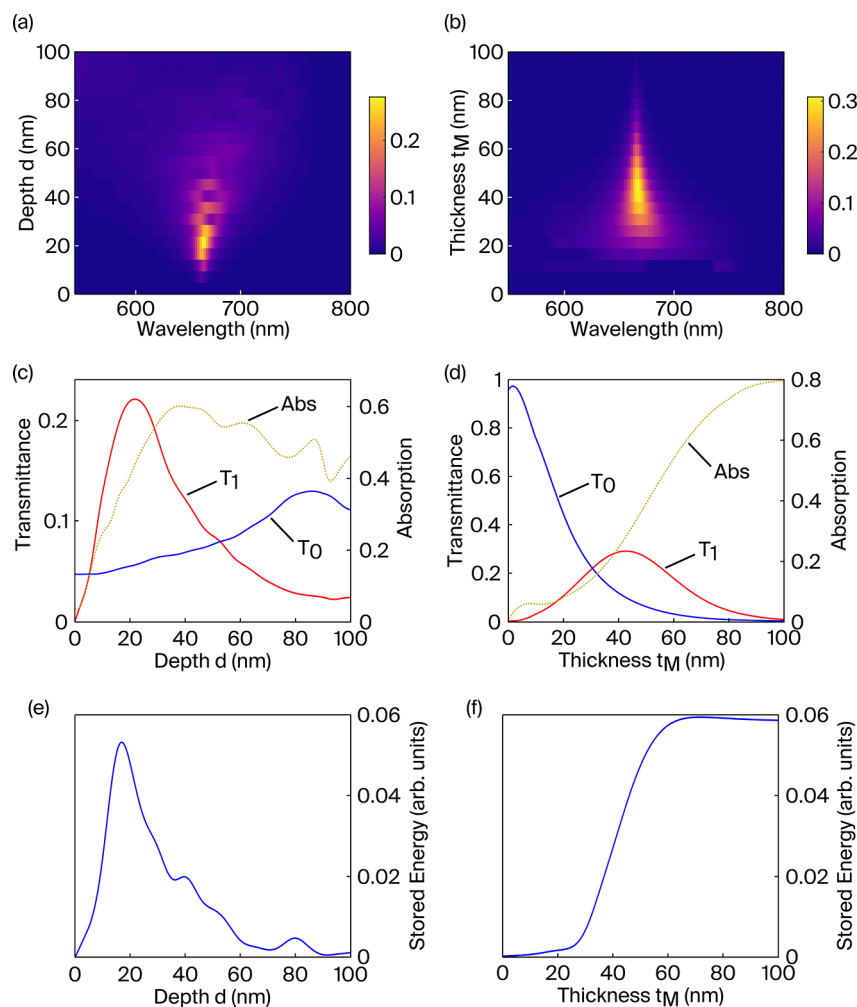
Figure 3. Simulated efficiency T_1 (a) for different grating depths d at t_M = 50 nm and (b) for different metal thicknesses t_M at d = 20 nm. Efficiencies T_1, T_0, and absorption are evaluated at the resonance peaks (c) for different grating depths d and (d) for different metal thicknesses t_M. The stored energy is evaluated as the ratio of reflectance R_0 at resonance (e) to the fwhm for different grating depths d and (f) for different metal thicknesses t_M. Other parameters are Λ = 500 nm, t_W = 80 nm.

We now would like to discuss the conditions under which the first order diffraction efficiency is maximized, and base our analysis on a Fano interference model. In a photonic system, a Fano interference is built between a mode and a continuum of freely propagating light.[23,35,36] In our case, the mode is bound to the metallic/dielectric thin waveguide. Unlike usual grating diffraction analysis, we consider here two continua T_{a_0} and T_{a_1}, consisting of the background zeroth and first order of diffraction, respectively. The zeroth and first order diffraction efficiencies around the resonance wavelength can be modeled by a Fano-like asymmetric line shape:[37,38]

$$T_{0,1} = T_{a_{0,1}} \frac{(\omega - \omega_0 + q\gamma)^2 + b\gamma^2}{(\omega - \omega_0)^2 + \gamma^2} \quad (3)$$

where ω_0 is the Fano resonance frequency, q the Fano asymmetry parameter, $\gamma = \gamma_c + \gamma_i$ the resonance width, γ_c and γ_i the radiative and the nonradiative damping, and $b = \gamma_i^2/\gamma^2$ the modulation damping. The amplitude of the transmission at resonance depends on the coupling between the mode and the continuum, the intrinsic losses as well as on the amplitude $T_{a_{0,1}}$ of the continuum itself. In the following we study by RCWA modeling the influence of two parameters on the T_1 response:

the grating depth d (Figure 3a) and the metallic layer thickness t_M (Figure 3b). Due to the staircase approximation in the RCWA model, a local regression of the results is performed using weighted linear least-squares and a first-degree polynomial model to minimize local lobes in the results of Figure 3c,d. The optimization has been performed by screening both grating depth and metal thickness together. The maximum T_1 efficiency is obtained for d = 25 nm and t_M = 50 nm.

The first order transmittance T_1 at resonance is compared to the zeroth order transmittance T_0 and the absorption at the same wavelength in Figure 3c,d. The corresponding variation of the stored energy, evaluated as the ratio between the reflectance R_0 at resonance and the fwhm, is reported in Figure 3e,f. The grating depth is mostly responsible for coupling between the mode and the continuum, while the metal thickness influences optical losses. For a fixed grating depth d, the zeroth order transmittance decreases monotonically while the absorption increases before reaching saturation (Figure 3d): the field cannot fully penetrate through the metallic film according to the Beer–Lambert law, while the modal field is increasingly present in the metallic film, thus increasing optical losses. Interestingly, the first order transmittance reaches a
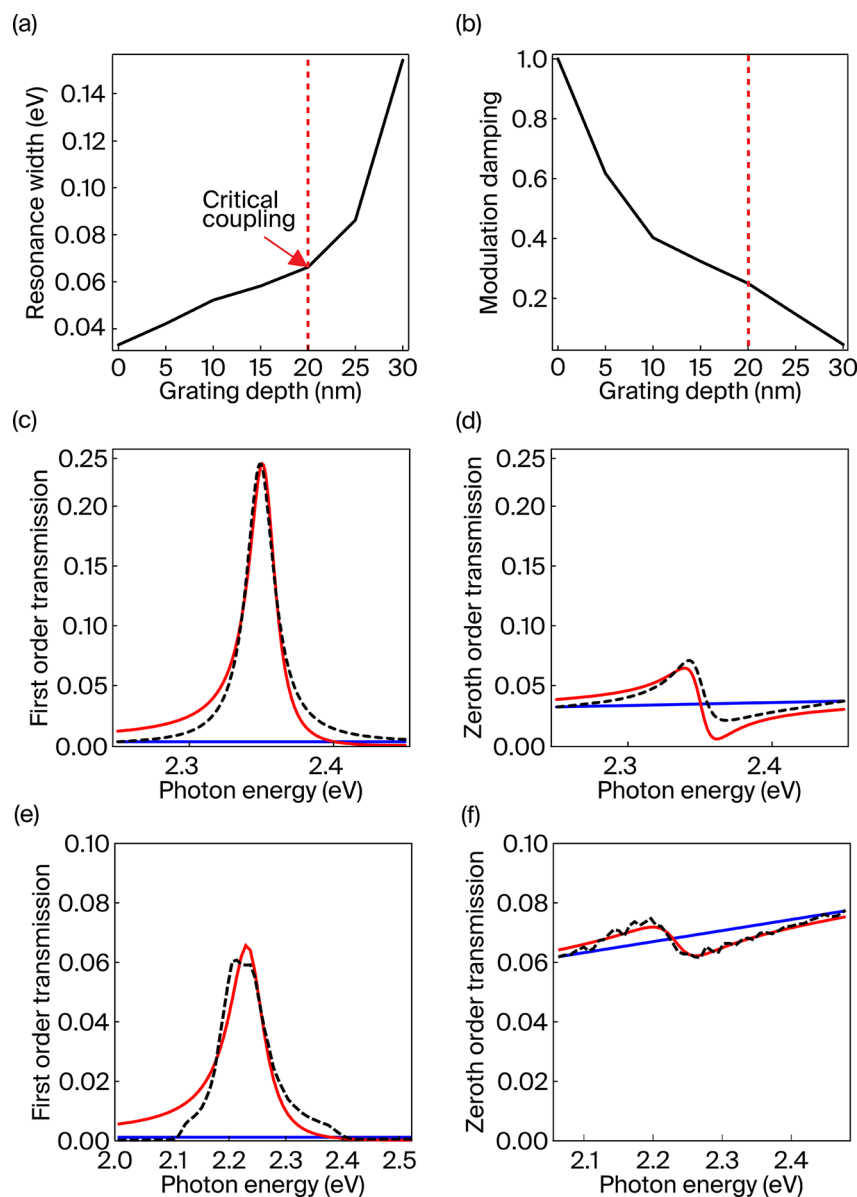
Figure 4. (a) Resonance width and (b) modulation depth fitted with eq 3 from simulated first order diffraction as a function of grating depth (Figure 3a). The critical coupling condition is characterized by a maximization of first order efficiency, resonance width $\gamma = 2\gamma_i$, and modulation damping $b = 1/4$. (c,d) Simultaneous fit of simulated (c) first and (d) zeroth order diffraction corresponding to Figure 1b. Dashed black: simulation. Solid red: fit with eq 3. Solid blue: intensity of continuum (c) T_{a_1} and (d) T_{a_0}. (e,f) Measured (e) first and (f) zeroth order diffraction of a device with period $\Lambda = 400$ nm, corrugation depth $d = 20$ nm and coating thicknesses $t_W = 40$ nm and $t_M = 80$ nm. Dashed black: simulation. Solid red: fit with eq 3. Solid blue: intensity of continuum (e) T_{a_1} and (f) T_{a_0}.

maximum value, which is a result of two separate effects. On one hand, a higher film thickness leads to an increase of the plasmon mode polarizability, and as a result to an increase of the resonance amplitude and the amplitude of the field released in the first order of diffraction. To confirm this interpretation, a monotonous increase of the modal stored energy is observed in Figure 3f. On the other hand, the amplitude of the continuum T_{a_1} exponentially decreases as a function of the thickness of the metallic layer according to the Beer–Lambert law. The resonance appears as an amplitude modulation of the continuum in eq 3, so the spectral behavior of the resonance and the continuum both contribute to the T_1 spectrum. The balance between the amplitude of the continuum, the plasmon excitation amplitude, and optical

losses determines a maximum in the first diffraction order transmission at $t_M = 50$ nm, which is consistent with other observations reported by Fang et al.[39] and by Giannattasio et al.[40] in the case without dielectric layer ($t_W = 0$ nm).

A different effect is observed when varying the grating depth for a fixed film thickness (Figure 3a,c,e). In this case, the modal stored energy, the first order transmission, and the absorption all reach a maximum. The amount of metallic material is constant and the depth is only weakly varied, so the intrinsic optical losses are approximately constant. On the other hand, the coupling efficiency is increased for increasing grating depth. Intrinsic losses and coupling efficiency are thus balanced at a specific value of the grating depth (here 20 nm), referred as a critical coupling condition in Fano-resonant systems.[41,42] In addition, constructive and destructive interferences in the

propagation of diffracted orders are observed, which are obtained when the grating modulation depth builds a difference in optical path length between the top and the bottom of the grating corrugation. The continuum of diffracted field $T_{a_{0,1}}$ is affected by these modulations, and as a result, the zeroth order transmission reaches a peak for a modulation depth of 90 nm. The first order maximum is also occurring at a slightly higher grating depth than the maximum in stored energy.

In order to quantitatively verify this interpretation, we perform fits of transmission spectra to eq 3. We follow an iterative approach where the resonance width and damping are first extracted, and their values fixed for fitting the asymmetry parameter q. It ensures extracting physically meaningful values of the resonance parameters. More specifically, a fit of the first order of transmission in Figure 3a to eq 3 has been performed for γ, q and b, assuming a constant background amplitude T_{a_1} given by the asymptotic value of the curve. The total resonance width γ can thus be extracted from this fit as a function of the grating depth (Figure 4a). The value of 0.033 eV for zero grating depth is obtained by linear extrapolation of the curve at low values of the grating depth, which corresponds by definition to a situation where only intrinsic losses are present (i.e., $\gamma = \gamma_i$). Since the curve is Lorentzian-like, similar values of the resonance width can be extracted with a fit to a Lorentzian. It is interesting to see that for the depth of 20 nm corresponding to critical coupling, we have $\gamma = 2\gamma_i$, i.e., $\gamma_c = \gamma_i$ implying that the external coupling balances intrinsic losses. Above critical coupling, a splitting of the resonance peak is observed and the fit accuracy decreases. We have then performed another fit for γ and q only, assuming a constant value of the intrinsic losses γ_i as the grating depth is increased. The resulting fitted modulation depth values b are shown in Figure 4b. Similarly to other Fano-resonance structures (see, e.g., ref 41), the critical coupling condition is also satisfied at $b = 1/4$. In general, the remaining asymmetry parameter q depends on a variety of effects, such as the relative background amplitude and phase, the resonance amplitude and phase, and the different optical loss channels. Therefore, it is here kept as a phenomenological parameter describing the resonance line shape.

Analyzing the response of a device with 20 nm modulation depth and period $\Lambda = 500$ nm (Figure 1b), we extract a resonance width $\gamma = 0.053$ eV and position $\omega_0 = 2.35$ eV, both from a fit to a Lorentzian or to eq 3 for the first order diffraction curve. We use the knowledge of Figure 4b to fix the value of b to 0.35 in the following, along with the resonance width and position. We also assume a linear background for the zeroth and first order of diffraction $T_{a_{0,1}}$, determined by their respective asymptotic values (solid blue curves in Figure 4c and d). We then perform a fit for the asymmetry parameter q for both the first order and zeroth order, shown as solid red curves in Figure 4c and d, respectively. For the first order of diffraction, we obtain $q = -8.8$, while we have only $q = -0.8$ for the zeroth order. This is fully consistent with the fact that the first order of diffraction profile is quasi-Lorentzian, while the zeroth order profile is asymmetric. Most importantly, this result shows that the zeroth order and first order of diffraction can be modeled with a Fano-like line shape, yielding the same resonance characteristics with only the asymmetry parameter q and continuum amplitudes being different. They have the same spectral line width because they result from the excitation of the same photonic mode. This effect is not restricted to hybrid waveguide modes. For example, Lawrence et al. report a narrowband light deflecting silicon metasurface with Fano resonances in the zeroth and first order of diffraction.[21] We can also note the presence of different degrees of asymmetries in their respective spectral lineshapes.

We are now interested in extracting the resonance parameters from experimental data, and relating the zeroth and first order of diffraction. We fabricated some devices with different grating periods and different grating depths. The fabrication involved the mastering of Si-wafers by electron beam lithography (Raith, EBPG5000ES) with ZEP resist and dry etching (Alcatel, AMS200SE). Each wafer had 8 different patterns of 1D gratings 3 mm × 3 mm, with periods from 300 nm to 1 μm. The wafers were etched at different depths, from 10 to 100 nm. Afterward, the patterns were transferred to SiO$_2$ substrates by UV-nanoimprint lithography, and then coated with Ag ($t_M = 50$ nm) and SiO$_2$ ($t_W = 80$ nm) layers by electron beam evaporation (Leybold Optics, LAB600H). We have then measured the first diffraction order transmission T_1 for one of those realizations. A broad-spectrum white light covering the whole visible and near-IR spectrum (400 to 1000 nm) was generated with a Halogen Lamp (DL-2000, Ocean Optics) and in-coupled into a fiber with NA = 0.15. The fiber was connected to a parabolic reflective collimator (RC04SMA, Thorlabs) and reduced in diameter with an aperture (3 mm). The system was placed on a motorized rotation stage (CR1-Z7, Thorlabs) to scan the transmission angle. A second motorized rotation stage was placed on top of the previous one. The sample was placed on that second stage with a holder in order to tune the incident angle of the collimated light on the sample. The system was then placed on a motorized linear stage (LTS300, Thorlabs) to achieve a higher alignment precision. A spectroradiometer (Spectrascan PR-730, Photo Research) was used to measure the transmitted light after the sample. A prism was glued with a refractive index matching liquid to the device to outcouple the T_1 scattered light. The transmitted light was recorded from 0° to 90° with steps of 0.5° with the numerical aperture of the spectroradiometer equivalent to 0.5°. The data was then normalized to air and the angular information converted from air to SiO$_2$ using Snell's law for comparison with simulations, and the efficiency increased with the Fresnel coefficients (by typically 18%) to take into account the losses at the prism/air interface.

An example of first order and zeroth order of diffraction measurements are shown in Figure 4e and f, respectively. Since the system is different from simulations, optical damping cannot be directly compared and the damping parameter will be considered as free. The first order transmission is fitted to eq 3 in Figure 4e, yielding a resonance width $\gamma = 0.166$ eV and position $\omega_0 = 2.235$ eV, which we use in the fit of the zeroth order Figure 4f. The damping parameter is 0.96 for both the first order and zeroth order of diffraction. A notable difference with respect to the simulations of Figure 4c,d is the relative amplitude of intrinsic losses, leading to a larger damping parameter and spectral bandwidth. Similarly to simulations, the asymmetry parameter takes different value for the first and zeroth order (-7.94 and -0.09, respectively), while the resonance bandwidth and position, damping parameter are common.

Now that the Fano-resonant nature of the system has been established, we would like to validate the proposed dispersion model of eq 1. Measurements have been performed on devices
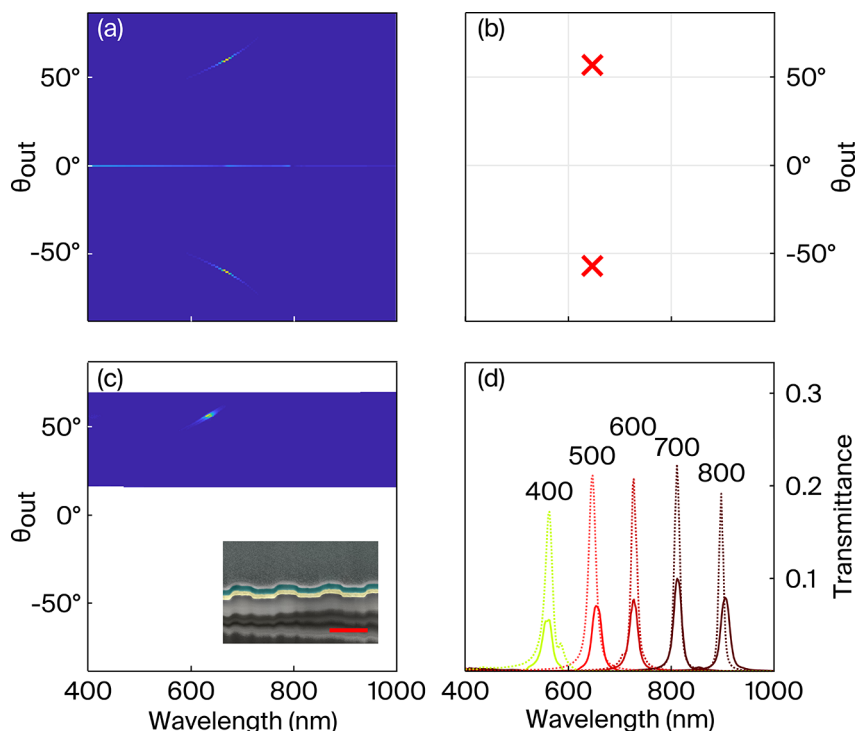
Figure 5. (a) Simulations, (b) analytical calculation, and (c) measurements of the first diffraction order transmittance T_1, integrated every 0.5°, for $\Lambda = 500$ nm. The inset in (c) shows an SEM image of the fabricated device, the scale bar is 500 nm long. The metallic layer is in yellow, the dielectric layer in bluish green. (d) Integrated transmittance T_1 around the diffracted peaks for the simulations (dashed lines) and measurements (solid lines) for devices with different grating periods. The parameters for the fabricated devices are $t_W = 80$ nm, $t_M = 50$ nm, $\Lambda = (400, 500, 600, 700, 800)$ nm.
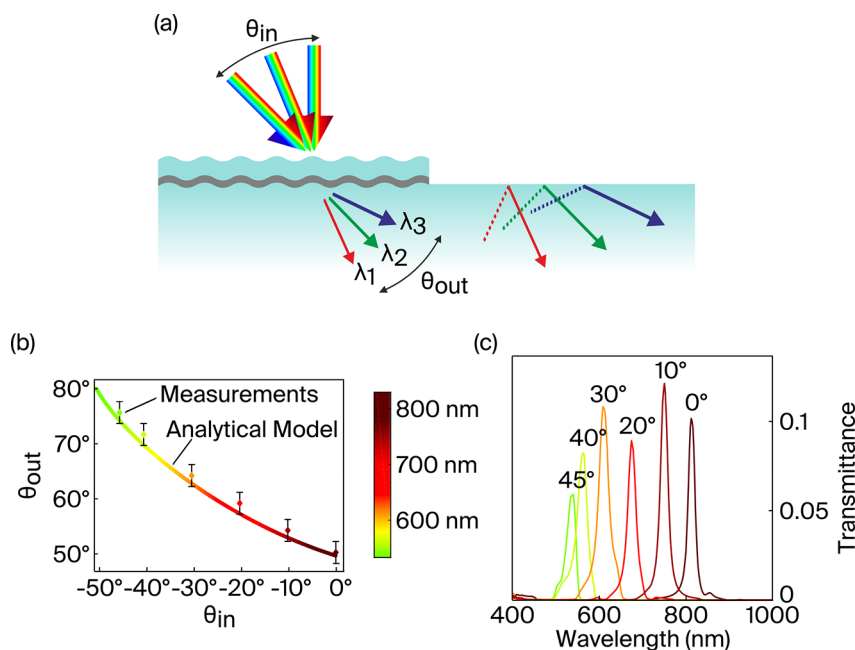
Figure 6. (a) Schematic of the angular dispersion θ_{out} of the device for different angles of incidence θ_{in} from 0° to 45°, where 0° defines an incidence normal to the substrate. (b) Calculated dispersion and measured first order diffraction transmittance T_1 at different incident angles θ_{in}. (c) Narrowband spectrum of the measured first order diffraction transmittance T_1. Parameters: $\Lambda = 700$ nm, $t_W = 80$ nm, $t_M = 50$ nm.

with different periods. The results are shown in Figure 5, with good agreement between the analytical model, RCWA simulations and measurements. For a given incidence angle, two peaks in the first and minus first order of diffraction are observed in the range of investigated angles and wavelengths

(Figure 5a). Their position is reproduced in the analytical model (Figure 5b) and numerical simulations (Figure 5c). The line in Figure 5a at $\theta_{out} = 0°$ corresponds to the zeroth order of transmission. The increase of resonance wavelength in the first order of diffraction with increasing periodicity can be clearly

seen. From Figure 2, the resonance position is dependent on the dielectric waveguide thickness t_W while it is not affected by the metal thickness t_M. The measurement of thin film thicknesses t_W and t_M is subject to an uncertainty estimated to approximately 10 nm. In addition, variations of the deposited film thickness across the measurement area can lead to a broadening of the resonance peak. Numerical simulations in Figure 5d have been performed considering a Gaussian distribution of thicknesses with nominal value of 67.5 nm and standard deviation of 2.5 nm. The chosen range of thicknesses are smaller than the target of 80 nm but within the range of thickness measurement uncertainty. The simulation including a thickness distribution also leads in average to a reduced peak amplitude, from approximately 0.3 to 0.2. Despite the above considerations, the lower measured efficiency remains smaller than simulations, a difference which can be attributed to the scattering by structural roughness during the propagation of the hybrid modes.

Finally, we investigate the angle dependency of the system in Figure 6. Due to the modal dispersion, the peak wavelength in first order is blue-shifted when the incidence angle is increased (Figure 6b,c). As a result, the diffraction angle is also increased. Measurements of the peak position are in good agreement with the analytical model (eq 1). When the incidence angle is increased, two different surface modes are excited at different wavelengths and propagate in opposite directions, leading to different contributions to the $T_{(+1)}$ and $T_{(-1)}$ diffraction orders. Overall, a shift of almost 300 nm of the resonance peak is observed when the incidence angle is increased from 0° to 45°. We propose in the schematic illustration in Figure 6a to use divergent sources to generate angularly and spectrally separated transmission peaks in the first order. This approach is fundamentally different from a standard diffraction grating, as in such situation the different wavelengths would angularly overlap. A photodetector can be placed for example at some distance from the waveguide coupler in order to collect the signal at different locations and extract a spectrum of the incident light. This way, a miniature spectrometer can be built and integrated in, e.g., consumer electronics devices. For sensing purposes, the shift of the Fano resonance wavelength for a perturbation of its immediate environment is particularly amplified at critical coupling.[42] Using the approach presented in Figure 6, this wavelength shift will directly result in a shift of the first order diffracted angle, which can be probed as a change of spatial distribution of the intensity with a photodetector placed at some distance after the waveguide coupler. An alternative sensing way in Fano-resonant system is based on the change of Fano modulation amplitude upon, e.g., a perturbation of the absorption in the vicinity of the resonant structure, where a very high sensitivity is observed below the critical coupling regime.[41,43] In the present case, a modulation of the peak intensity would be probed at a constant wavelength. Thus, the orthogonality in the sensing signal between a perturbation of the refractive index and of the absorption can be retrieved using the approach of Figure 6 as these perturbations respectively result in a change of signal position and intensity on the photodetector. We therefore conclude that narrowband diffraction can be exploited in a variety of applications, as this approach takes advantages from both plasmonic and photonic structures.

■ SUMMARY

We have reported on a resonant waveguide nanostructure performing narrowband first order diffraction with a quasisuppressed background amplitude. This effect relies on the excitation of hybrid plasmonic and waveguide modes, for which a semianalytical model has been developed and validated against numerical calculations and experiments. The incident light is incoupled in the thin film metallic dielectric structure by first order diffraction, propagates as a hybrid mode, and is released by evanescent coupling in the multimode light guide. The modal dispersion and thus the diffraction angle can be tailored with the waveguide film parameters, which goes beyond the sole use of grating periodicity. A model based on Fano resonances considering two different continuua, the nonresonant zeroth order and first order of diffraction, has been proposed. An analysis of the modal energy storage, the first order and zeroth order transmission, and absorption as a function of the grating depth and metal thickness has revealed a critical coupling regime at which the modal energy and first order efficiency is maximized. The model has been validated on simulation and experimental data, and shown in particular that the resonance profile of the zeroth and first order of diffraction have a similar resonance width, position and depth, while they differ in the Fano asymmetry parameter q. Fabrication of devices has been performed with UV nanoimprint lithography and thin film coatings. The measured peak positions are in good spectral agreement with modeling. The reported fwhm is of 10 nm in simulations and 20 nm in measurements of first order diffraction. Finally, we have investigated the angle dependency of the structures. Due to its dispersion, a shift of the peak wavelength is observed as a function of incidence the angle. Thus, divergent sources can be used to generate angularly and spectrally separated transmission peaks in the first order.

Thanks to its ease of fabrication, which requires only one nanoimprint step and two evaporation steps, the coupler is fully compatible with large scale industrial applications. It is further possible to engineer devices that share the same materials and layers thicknesses but have different wavelength incoupled, by having different grating periods. Further developments could rely on 2D gratings or advanced patterns, to improve the efficiency under unpolarized light and achieve higher angular tunability. Their efficiency could be increased by having a tilted evaporation of the metallic layer or using blazed gratings[44] or by exploiting long-range SPPs with thinner metallic layers. The study of this system under TE polarized light could also be of interest, because the resonance-induced absorption can produce even narrower features for the same geometry without surface plasmon resonances.[45] The device can also be implemented in a reciprocal configuration to outcouple light from a multimode waveguide. Applications are foreseen in many optical devices that require color-selective coupling or dispersive properties, such as optical document security or near-eye displays. Moreover, the dispersion behavior under divergent light source can be utilized to design inexpensive, compact, and robust spectrometers or biosensors.

The reported analysis method based on a general Fano formalism can be utilized for the optimization of narrowband diffraction devices, resonant waveguide gratings, and metasurfaces. Intrinsic losses are related to material absorption or can be modeled as a consequence of fabrication imperfections leading to inhomogeneous broadening. The understanding of

the interplay between optical coupling and intrinsic losses is of prime importance to optimize the efficiency, especially in the near-infrared and visible ranges where the weight of intrinsic losses is relatively high. Sensors based on modification of absorption in guided mode resonances can also benefit from this study to enhance their signal-to-noise ratio.[43,46]

■ ASSOCIATED CONTENT

Ⓢ Supporting Information

The Supporting Information is available free of charge at https://pubs.acs.org/doi/10.1021/acsphotonics.1c00072.

> S.1: Derivation of the dispersion relation of a four-layer slab waveguide (eq 1); S.2: Influence of incidence angle on minus first order diffraction (PDF)

■ AUTHOR INFORMATION

Corresponding Author

Benjamin Gallinet − *CSEM SA, Muttenz Center, Muttenz 4132, Switzerland;* ⓞ orcid.org/0000-0001-7444-3398; Email: benjamin.gallinet@csem.ch

Authors

Giorgio Quaranta − *CSEM SA, Muttenz Center, Muttenz 4132, Switzerland; EPFL Lausanne, Nanophotonics and Metrology Laboratory, Lausanne 1015, Switzerland;* Present Address: (G.Q.) SUSS MicroOptics SA, Rouges-Terres 61, Hauterive 2068, Switzerland; ⓞ orcid.org/0000-0003-3471-3802

Fabian Lütolf − *CSEM SA, Muttenz Center, Muttenz 4132, Switzerland;* ⓞ orcid.org/0000-0002-1938-8952

Olivier J. F. Martin − *EPFL Lausanne, Nanophotonics and Metrology Laboratory, Lausanne 1015, Switzerland;* ⓞ orcid.org/0000-0002-9574-3119

Complete contact information is available at:
https://pubs.acs.org/10.1021/acsphotonics.1c00072

Notes

The authors declare no competing financial interest.

■ ACKNOWLEDGMENTS

■ REFERENCES

(1) Asghari, M.; Krishnamoorthy, A. V. Energy-efficient communication. *Nat. Photonics* **2011**, *5*, 268−270.

(2) Avrutsky, I. A.; Svakhin, A. S.; Sychugov, V. A.; Parriaux, O. High-efficiency single-order waveguide grating coupler. *Opt. Lett.* **1990**, *15*, 1446−1448.

(3) Xiao, Z.; Liow, T.-Y.; Zhang, J.; Shum, P.; Luan, F. Bandwidth analysis of waveguide grating coupler. *Opt. Express* **2013**, *21*, 5688−5700.

(4) Wang, J. Chip-scale optical interconnects and optical data processing using silicon photonic devices. *Photon. Netw. Commun.* **2016**, *31*, 353−372.

(5) Quaranta, G.; Basset, G.; Martin, O. J. F.; Gallinet, B. Recent Advances in Resonant Waveguide Gratings. *Laser Photonics Reviews* **2018**, *12*, 1800017.

(6) Fan, S. H.; Joannopoulos, J. D. Analysis of Guided Resonances in Photonic Crystal Slabs. *Phys. Rev. B: Condens. Matter Mater. Phys.* **2002**, *65*, 235112.

(7) Bonod, N.; Enoch, S.; Li, L.; Popov, E.; Nevière, M. Resonant optical transmission through thin metallic films with and without holes. *Opt. Express* **2003**, *11*, 482−490.

(8) Genet, C.; Ebbesen, T. W. Light in Tiny Holes. *Nature* **2007**, *445*, 39−46.

(9) Sauvage-Vincent, J.; Tonchev, S.; Veillas, C.; Reynaud, S.; Jourlin, Y. Optical security device for document protection using plasmon resonant transmission through a thin corrugated metallic film embedded in a plastic foil. *J. Eur. Opt. Soc., Rapid Publ.* **2013**, DOI: 10.2971/jeos.2013.13015.

(10) Burgos, S. P.; Yokogawa, S.; Atwater, H. A. Imaging via Nearest Neighbor Hole Coupling in Plasmonic Color Filters Integrated Onto a Complementary Metal-Oxide Semiconductor Image Sensor. *ACS Nano* **2013**, *7*, 10038−10047.

(11) Mejía-Salazar, J. R.; Oliveira, O. N. Plasmonic Biosensing. *Chem. Rev.* **2018**, *118*, 10617−10625.

(12) Kress, B. C.; Cummings, W. J. Towards the Ultimate Mixed Reality Experience: HoloLens Display Architecture Choices. *Dig. Tech. Pap. - Soc. Inf. Disp. Int. Symp.* **2017**, *48*, 127−131.

(13) Levola, T.; Laakkonen, P. Replicated slanted gratings with a high refractive index material for in and outcoupling of light. *Opt. Express* **2007**, *15*, 2067−2074.

(14) Lütolf, F.; Stalder, M.; Martin, O. J. F. Up-scalable method to amplify the diffraction efficiency of simple gratings. *Opt. Lett.* **2014**, *39*, 6557−6560.

(15) Lalanne, P.; Astilean, S.; Chavel, P.; Cambril, E.; Launois, H. Blazed binary subwavelength gratings with efficiencies larger than those of conventional échelette gratings. *Opt. Lett.* **1998**, *23*, 1081−1083.

(16) Aieta, F.; Kats, M. A.; Genevet, P.; Capasso, F. Multiwavelength achromatic metasurfaces by dispersive phase compensation. *Science* **2015**, *347*, 1342−1345.

(17) Lin, D.; Melli, M.; Poliakov, E.; Hilaire, P. S.; Dhuey, S.; Peroz, C.; Cabrini, S.; Brongersma, M.; Klug, M. Optical metasurfaces for high angle steering at visible wavelengths. *Sci. Rep.* **2017**, *7*, 2286.

(18) Campbell, S. D.; Sell, D.; Jenkins, R. P.; Whiting, E. B.; Fan, J. A.; Werner, D. H. Review of numerical optimization techniques for meta-device design. *Opt. Mater. Express* **2019**, *9*, 1842−1863.

(19) Sell, D.; Yang, J.; Doshay, S.; Yang, R.; Fan, J. A. Large-Angle Multifunctional Metagratings Based on Freeform Multimode Geometries. *Nano Lett.* **2017**, *17*, 3752−3757.

(20) Klopfer, E.; Lawrence, M.; Barton, D. R.; Dixon, J.; Dionne, J. A. Dynamic Focusing with High-Quality-Factor Metalenses. *Nano Lett.* **2020**, *20*, 5127−5132.

(21) Lawrence, M.; Barton, D. R., III; Dixon, J.; Song, J.-H.; van de Groep, J.; Brongersma, M. L.; Dionne, J. A. High quality factor phase gradient metasurfaces. *Nat. Nanotechnol.* **2020**, *15*, 956.

(22) Overvig, A. C.; Malek, S. C.; Yu, N. Multifunctional Nonlocal Metasurfaces. *Phys. Rev. Lett.* **2020**, *125*, 017402.

(23) Miroshnichenko, A. E.; Flach, S.; Kivshar, Y. S. Fano Resonances in Nanoscale Structures. *Rev. Mod. Phys.* **2010**, *82*, 2257−2298.

(24) Luk'yanchuk, B.; Zheludev, N. I.; Maier, S. A.; Halas, N. J.; Nordlander, P.; Giessen, H.; Chong, C. T. The Fano Resonance in Plasmonic Nanostructures and Metamaterials. *Nat. Mater.* **2010**, *9*, 707−715.

(25) Limonov, M. F.; Rybin, M. V.; Poddubny, A. N.; Kivshar, Y. S. Fano Resonances in Photonics. *Nat. Photonics* **2017**, *11*, 543−554.

(26) Burke, J. J.; Stegeman, G. I.; Tamir, T. Surface-polariton-like waves guided by thin, lossy metal films. *Phys. Rev. B: Condens. Matter Mater. Phys.* **1986**, *33*, 5186−5201.

(27) Sannikov, D. G.; Sementsov, D. I. The surface mode of a dielectric waveguide with metal substrate. *Tech. Phys. Lett.* **2003**, *29*, 353−356.

(28) Genet, C.; van Exter, M. P.; Woerdman, J. P. Fano-Type Interpretation of Red Shifts and Red Tails in Hole Array Transmission Spectra. *Opt. Commun.* **2003**, *225*, 331.

(29) Malitson, I. H. Interspecimen Comparison of the Refractive Index of Fused Silica*,†. *J. Opt. Soc. Am.* **1965**, *55*, 1205−1209.

(30) Yang, H. U.; D'Archangel, J.; Sundheimer, M. L.; Tucker, E.; Boreman, G. D.; Raschke, M. B. Optical dielectric function of silver. *Phys. Rev. B: Condens. Matter Mater. Phys.* **2015**, *91*, 235137.

(31) Moharam, M. G.; Gaylord, T. K. Rigorous coupled-wave analysis of planar-grating diffraction. *J. Opt. Soc. Am.* **1981**, *71*, 811−818.

(32) Lalanne, P.; Morris, G. M. Highly improved convergence of the coupled-wave method for TM polarization. *J. Opt. Soc. Am. A* **1996**, *13*, 779−784.

(33) Li, L. Use of Fourier series in the analysis of discontinuous periodic structures. *J. Opt. Soc. Am. A* **1996**, *13*, 1870−1876.

(34) Popov, E.; Nevière, M.; Gralak, B.; Tayeb, G. Staircase approximation validity for arbitrary-shaped gratings. *J. Opt. Soc. Am. A* **2002**, *19*, 33−42.

(35) Fano, U. Some theoretical considerations on anomalous diffraction gratings. *Phys. Rev.* **1936**, *50*, 573.

(36) Fano, U. The theory of anomalous diffraction gratings and of quasi-stationary waves on metallic surfaces (Sommerfeld's waves). *J. Opt. Soc. Am.* **1941**, *31*, 213−222.

(37) Gallinet, B.; Martin, O. J. F. Ab Initio Theory of Fano Resonances in Plasmonic Nanostructures and Metamaterials. *Phys. Rev. B: Condens. Matter Mater. Phys.* **2011**, *83*, 235427.

(38) Gallinet, B.; Martin, O. J. F. Influence of Electromagnetic Interactions on the Line Shape of Plasmonic Fano Resonances. *ACS Nano* **2011**, *5*, 8999−9008.

(39) Fang, N.; Liu, Z.; Yen, T.-J.; Zhang, X. Regenerating evanescent waves from a silver superlens. *Opt. Express* **2003**, *11*, 682−687.

(40) Giannattasio, A.; Hooper, I. R.; Barnes, W. L. Transmission of light through thin silver films via surface plasmon-polaritons. *Opt. Express* **2004**, *12*, 5881−5886.

(41) Gallinet, B.; Siegfried, T.; Sigg, H.; Nordlander, P.; Martin, O. J. F. Plasmonic Radiance: Probing Structure at the Angstrom Scale with Visible Light. *Nano Lett.* **2013**, *13*, 497−503.

(42) Gallinet, B.; Martin, O. J. F. Refractive Index Sensing with Subradiant Modes: A Framework To Reduce Losses in Plasmonic Nanostructures. *ACS Nano* **2013**, *7*, 6978−6987.

(43) Davoine, L.; Paeder, V.; Basset, G.; Schnieper, M.; Herzig, H. P. Resonant absorption of a chemically sensitive layer based on waveguide gratings. *Appl. Opt.* **2013**, *52*, 340−349.

(44) Lütolf, F.; Martin, O. J. F.; Gallinet, B. Fano-resonant aluminum and gold nanostructures created with a tunable, up-scalable process. *Nanoscale* **2015**, *7*, 18179−18187.

(45) Chen, W.; Guo, L.; Sun, Z. Resonant Absorption of TE-Polarized Light at the Surface of a Dielectric-Coated Metal Grating. *IEEE Photonics J.* **2014**, *6*, 1−6.

(46) Wang, Y.; Huang, Y.; Sun, J.; Pandey, S.; Lu, M. Guided-mode-resonance-enhanced measurement of thin-film absorption. *Opt. Express* **2015**, *23*, 28567−28573.